Using Pseudotime Marching for the Solution of Harmonic Balance Problems

Christian Frey[1]
Jan Backhaus
Graham Ashcroft
Georg Geiser
Institute of Propulsion Technology
German Aerospace Center (DLR)
Linder Höhe
51147 Cologne
Germany
christian.frey@dlr.de

Benjamin Winhart
MTU Aero Engines
Dachauer Str. 665
80995 Munich
Germany

Heinrich Stüer
Siemens Energy
Rheinstr. 100
45478 Mülheim a. d. Ruhr
Germany

The aim of this paper is to study approaches to implement implicit pseudotime marching for the harmonic balance system in the frequency domain. We first give a motivation for using pseudotime marching as a solution technique. It turns out that, when the discretization errors of the pseudospectral time derivative and the pseudotime derivative are neglected, the harmonic balance solution converges to a stable periodic flow, provided that the initial solution is sufficiently close to a stable periodic solution. This motivates the choice of a robust pseudotime marching approach, e.g., an implicit solver based on backward Euler integration. This approach requires the Jacobian of the harmonic balance residual. As for the steady problem, the Jacobian can be approximated without changing the final solution as long as the solver converges. Therefore, a central question is which simplifications are appropriate in terms of the overall efficiency and robustness of the solver.

As has been shown in the literature, the spectral time-derivative operator should be taken into account in the implicit system. On the other hand, the linearization of the flow residual can be simplified to a certain extent, especially if the system is solved in the frequency domain. In this paper, we show that, up to terms which scale with the amplitude of the disturbances, the linear system matrix is the sum of a scalar diagonal and a block diagonal matrix with identical blocks for each harmonic. The deviation from this structure is due to to the nonlinearity of the unsteady flow problem. We show that when the unsteadiness is small, the nonlinear coupling terms can be neglected in the implicit solver and the resulting special matrix structure can be exploited to massively speed up the solver. In contrast, when a strong disturbance is simulated, this simplification can lead to significant losses in robustness. To illustrate our findings we apply the implemented methods to predict the flow response to a disturbance prescribed at the inlet of a transonic compressor. When the disturbance amplitude is increased, a strong oscillation is induced, and the harmonic balance solver converges only when the nonlinear coupling between the harmonics is taken into account.

Keywords: unsteady flows, CFD methods, aeroelasticity, harmonic balance, pseudotime marching

1 Introduction

As CPU costs of predicting nonlinear unsteady aerodynamics in turbomachinery are becoming more and more affordable, complex flow phenomena that are not yet fully understood can now be analyzed using CFD. For a number of unsteady problems such as noise transmission or the onset of flutter, nonlinear flow physics may be relevant for the modeling of the background flow but not for the unsteady phenomena itself. However, there are highly relevant flow phenomena for which nonlinear mechanisms are critical for the unsteady dynamics themselves. These include, among others, the following:

- rotor-stator interactions and their impact on aerodynamic performance,
- asymmetric inflows and the influence on the aerodynamic performance,
- forced response due to rotor-stator interactions,
- flutter-induced limit cycles,
- self-induced flow instabilities,
- nonsynchronous vibrations,
- rotating stall.

The impact of these effects on performance, operating ranges or high-cycle fatigue of a turbomachinery component can be severe. The aim of this work is to find an appropriate CFD method which is, on the one hand, sufficiently fast and robust to be run in an industrial design loop and, on the other, taking relevant nonlinear effects into account. We focus on periodic unsteady phenomena, a category that includes many unsteady phenomena relevant to turbomachinery applications.

The harmonic balance (HB) technique which, in the turbomachinery CFD community, was introduced over 20 years ago by Hall et al. [1] is a natural choice, as it has been demonstrated by many researchers to considerably reduce CPU times for time-periodic problems. In this work, we address the question of how to implement efficient and robust solution methods for the HB system.

Whereas for the simulation of nonlinear electric circuits [2,3] and structural dynamics [4], Newton methods are quite common for the solution of the HB system, nearly all HB solvers in CFD use pseudotime marching thereby generalizing the common approach for steady solvers [1]. The pseudotime term was added to the harmonic balance equations in a rather ad-hoc manner without much justification other than the observation that it made the HB system resemble the steady pseudotime equation. The main difference, it seemed, were the time-derivative terms which many authors regarded as "HB source terms".

Woodgate and Badcock [5] presented an implicit pseudotime solver for the harmonic balance equations. The solver as well as the

[1]Corresponding Author.
January 4, 2025

implicit linear system were formulated in the time-domain, so that the linearization of the time-derivative was the only term that coupled the sampling points. Numerical experiments showed that these off-diagonal terms could not be dropped from the harmonic balance Jacobian, with significant implications for the memory requirements of the method. Su and Yuan [6] also implemented a fully implicit harmonic balance solver. For a classical LU-SGS they observed reduced robustness and attributed the numerical stability issues to the loss of diagonal dominance in the time-domain formulation due to the addition of the spectral time-derivative. As did Woodgate and Badcock, they proposed to implement a preconditioned Krylov method as approximate linear solver. Sicot et al. [7] reported convergence issues when LU-SSOR was applied to the fully implicit HB system. They suggested the use of the so-called *Block-Jacobi Successive Overrelaxation* method. There are successful attempts in the literature to analyze the HB systems by means of its spectrum and draw conclusion about how to develop implicit methods. For instance, Thomas et al. [8] showed that neglecting the so-called HB source term in the linear system will result in an unstable system for very short and very long wavelengths which explained the behavior observed in previous studies. The authors then showed that a two-step approximate factorization, in which the system is temporally (first step) or spatially (second step) decoupled results in an unconditionally stable iterative scheme.

Summarizing, all attempts to generalize implicit steady methods by neglecting the time-derivative in the implicit linear systems were reported to reduce the computational effort while at the same time causing considerable instabilities. In this paper, we revisit the problem of formulating implicit formulations for pseudotime marching solvers of the HB system. The main difference with the work cited above is that the HB solver here is formulated in the frequency domain. One of the goals of this work is to show that in most practical situations one can drop the off-diagonal terms which, in contrast to the time-domain solvers, couple the harmonics and, as is shown below, scale with the nonlinearity of the problem. This is in stark contrast with the time-domain systems, for which the work by Thomas et al. [8] showed that even for infinitesimal amplitudes, dropping the off-diagonal terms (that couple the time instants) may result in unstable pseudotime dynamics.

To support our findings, we study a transonic compressor test case where, near the numerical stall margin, unsteady disturbances are prescribed at the inlet. By scaling the disturbances we are able to artificially increase the unsteady amplitudes. The results illustrate that dropping the coupling between the harmonics comes at the expense of robustness. In contrast to the decoupling of time instants, however, the decoupling of harmonics is found to result in a severe loss of stability only in the case of extremely high amplitudes.

Furthermore, we give in this paper, for the first time in the open literature, a concise mathematical argument why the pseudo-time approach for the harmonic balance method should, at least in the limit of many harmonics and small pseudotime steps, give similar results as a time-domain URANS solver even for strongly nonlinear dynamics.

2 Harmonic Balance

The harmonic balance method which is investigated in this paper is part of the flow solver TRACE [9]. TRACE has been developed for more than three decades by DLR in close cooperation with MTU Aero Engines. Originally developed as a finite-volume based code for the compressible Reynolds-Averaged Navier-Stokes (RANS) equations, the flow solver has in recent years been extended to include modules for simulating combustion [10], adjoint based optimization [11], and discontinuous Galerkin methods [12]. In the present work we use the finite-volume method to discretize the compressible RANS equations with Roe's upwind scheme [13], MUSCL extrapolation [14], and a van Albada-type limiter [15]. For the simulation results presented below, Wilcox' k-ω turbulence model [16] with the Kato-Launder modification [17] was used.

The harmonic balance solver employs the alternating frequency time-domain (AFT) approach, i.e., we compute the spectral time-derivative in the frequency domain whereas the flow residuals are evaluated for a set of sampling points at which the flow is reconstructed with an inverse discrete Fourier transform, the matrix of which will be denoted by F^{inv}. Denoting by K the number of higher harmonics and $N \geq 2K+1$ the number of sampling points t_n, $n = 0, ..., N-1$, the solution at the n-th sampling point is thus

$$q_n = \Re \sum_{k=0}^{K} \widehat{q}_k e^{\mathbf{i}\omega_k t_n} = F^{\text{inv}}_{nk} \widehat{q}_k. \tag{1}$$

In this paper, we assume that the frequencies are $\omega_k = k\omega$, for $k = 0, ..., K$ and that the sampling points are uniformly distributed over the period,

$$t_n = \frac{n}{N} \cdot \Delta t, \quad \Delta t = \frac{2\pi}{\omega}$$

The harmonic balance system in the frequency domain is thus

$$R^{\text{HB}}(\widehat{q}) = 0, \tag{2}$$

where the harmonic balance residual R^{HB} is the vector whose k-th component is

$$R^{\text{HB}}_k = \mathbf{i}k\omega\widehat{q}_k + \widehat{R(q)}_k, \quad q = F^{\text{inv}}\widehat{q}. \tag{3}$$

The Fourier coefficients of the flow residuals are computed using the discrete Fourier transform, the corresponding matrix of which is denoted by F.

The number of sampling points N is set to $N = (n_{\text{hh}} - 1)K + 1$ with K denoting the highest harmonic. n_{hh}, the number of sampling points per period for the highest harmonic. $n_{\text{hh}} = 3$ is the lower limit for the number of sampling points and corresponds to the Nyquist criterion. $n_{\text{hh}} = 4$ is the minimum value to guarantee that taking products of two harmonics does not result in a mode which is indistinguishable from some original harmonic, i.e., aliasing [18]. For the simulations below $n_{\text{hh}} = 5$ has been used which suppresses aliasing due to cubic nonlinearities and which results in $N = 4K+1$ sampling points. Note that in the case of oversampling, i.e., if $N > 2K+1$, F is the pseudoinverse of F^{inv}.

For applications with multiple fundamental frequencies, the solver has been extended based on the so-called *harmonic set* approach [19] and multidimensional-time harmonic balance [20]. These extensions, however, are outside the scope of this work. The nonreflecting boundary conditions as well as the blade row coupling method can be found in [21].

3 Pseudotime Solver

The pseudotime marching technique consists in the integration of the ordinary differential equation system

$$\frac{\partial \widehat{q}_k}{\partial \tau} + \mathbf{i}\omega k\widehat{q}_k + \widehat{R(q)}_k = 0, \quad k = 0, ..., K. \tag{4}$$

Note that, since R is nonlinear, the k-th harmonic of the residual R will, in general, depend on all harmonics of q which implies that Eq. (4) is a coupled system. Apply the inverse Fourier transform F^{inv} to Eq. (4) to obtain

$$\frac{\partial q_n}{\partial \tau} + (D_t q)_n + (\Pi_K R(q))_n = 0, \quad n = 0, ..., N-1. \tag{5}$$

Here, D_t is the spectral time derivative

$$D_t = F^{\text{inv}} \begin{pmatrix} 0 & 0 & \cdots & 0 \\ 0 & \mathbf{i}\omega & \cdots & 0 \\ \vdots & \vdots & \ddots & \vdots \\ 0 & 0 & \cdots & \mathbf{i}K\omega \end{pmatrix} F, \tag{6}$$

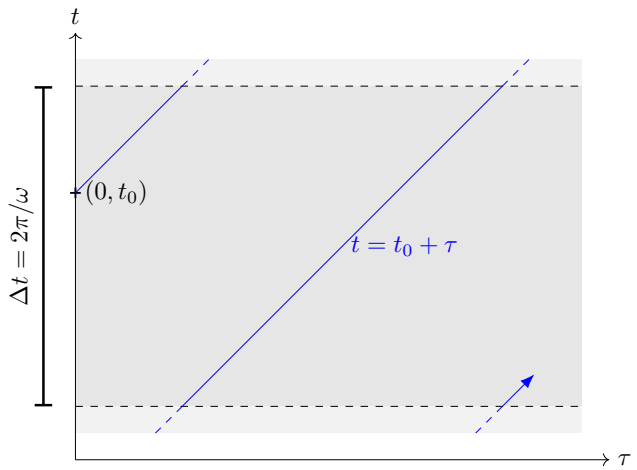

Fig. 1 Integral curve of the vector field corresponding to the sum of pseudotime-time and time derivatives.

usually encountered in time-domain formulations of harmonic balance solvers (e.g. [1]). The operator Π_K represents the modal filter onto the solution space, i.e., the flow solutions along the N sampling points which can be reconstructed from up to K higher harmonics,

$$\Pi_K = F^{\text{inv}} F. \tag{7}$$

If no oversampling is used, then $N = 2K+1$ and Π_K is the identity operator, so Eq. (5) then takes exactly the form of the pseudotime marching of the time-domain harmonic balance (or "time-spectral") solvers, cf. [1,8].

It follows that the pseudotime marching harmonic balance solvers, regardless of whether they are modal or nodal in time, implement a discretization of the partial differential equation

$$\frac{\partial q}{\partial \tau} + \frac{\partial q}{\partial t} + R(t, q) = 0, \quad q(0, t) = q^0(t) \tag{8}$$

where $q(\tau, t)$ represents a spatially discretized solution which is Δt-periodic in t. $q^0(t)$ is the initial solution used to start the pseudotime solver, typically a solution to a steady problem. We have added the time-dependence of R as we are primarily interested in non-autonomous problems, i.e., the unsteadiness is due to a relative rotation, a blade vibration or an unsteady inhomogeneous boundary condition. Now, Eq. (8) can be viewed as a system of transport equations in the τ-t-plane whose characteristic curves are given by $t = t_0 + \tau$. Figure 1 depicts such a line in the rectangular domain

$$\{(\tau, t) \,|\, \tau \geq 0, \quad 0 \leq t \leq \Delta t\}$$

with periodic boundaries in the t-direction. The characteristic lines could also be depicted as helices inclined by 45° against the τ = const planes if the t-periodic functions along the rectangular domain above are thought of as functions along a semi-cylinder. The following arguments, however, are simplified if one imagines the solution space as Δt-periodic functions in t defined on the whole half-plane $\tau \geq 0$.

Consider a solution $q(\tau, t)$ to the semi-discrete system in Eq. (8),

$$\left(\frac{\partial}{\partial \tau} + \frac{\partial}{\partial t}\right) q(\tau, t) + R(t, q(\tau, t)) = 0, \quad q(0, t) = q^0(t). \tag{9}$$

For $t_0 \in \mathbb{R}$, define a single time-parameter function by

$$\tilde{q}_{t_0}(t) = q(t - t_0, t), \quad t \geq t_0$$

This is the restriction of the solution to a characteristic line. It is straightforward to check that

$$\begin{aligned}
\frac{\partial \tilde{q}_{t_0}}{\partial t}\Big|_t &= \frac{\partial q}{\partial \tau}\Big|_{(t-t_0,t)} + \frac{\partial q}{\partial t}\Big|_{(t-t_0,t)} \\
&= \left(\frac{\partial}{\partial \tau} + \frac{\partial}{\partial t}\right) q(t - t_0, t) \\
&= -R(t, q(t - t_0, t)) \\
&= -R(t, \tilde{q}_{t_0}(t)),
\end{aligned}$$

so $\tilde{q}_{t_0}$ is the solution to the semi-discrete URANS equation,

$$\frac{\partial \tilde{q}_{t_0}}{\partial t} + R(t, \tilde{q}_{t_0}(t)) = 0, \tag{10}$$

with initial value given by the solution value of the initial solution q^0 at t_0 since

$$\tilde{q}_{t_0}(t_0) = q(0, t_0) = q^0(t_0).$$

Hence, the harmonic balance solution along the characteristics $t = t_0 + \tau$ corresponds to a solution of the semi-discrete URANS equations. Therefore, if for the given initial value, the solutions of the URANS equations approach a Δt-periodic solution, $q^*(t)$ say, then the harmonic balance solution satisfies

$$\|q(t - t_0, t) - q^*(t)\| = \|\tilde{q}_{t_0}(t) - q^*(t)\| \underset{t\to\infty}{\longrightarrow} 0.$$

The harmonic balance solution will therefore approach q^* for $\tau \to \infty$. Conversely, if the harmonic balance solution approaches a time-periodic flow q^*, then so do the solutions of the semi-discrete URANS system for all initial values $q^0(t_0)$, $0 \leq t_0 < \Delta t$. Summarizing, if we neglect the discretization errors of the pseudotime and time derivatives, then the harmonic balance solution converges to a limit cycle for $\tau \to \infty$ if and only if the URANS solutions do for $t \to \infty$, provided both systems are initialized consistently.

The above argument requires the pseudotime and time derivatives to be exact, but nevertheless suggests that if the discretization errors are small (e.g. using small pseudo-time steps and large numbers of harmonics), it should be possible to compute exactly those periodic solutions that can be simulated with a standard URANS approach. It also points to the fact that if the time-integration method does not approach a periodic solution (e.g., in the case of quasi-periodicity or chaos), a similar behavior should be expected for the harmonic balance solution along the lines $t = t_0 + \tau$. Moreover, we will see below, that simplifying assumptions during the τ-discretization can indeed cause divergence of the HB solver and may severely limit the pseudotime step size.

The analogy above is a sound heuristic argument why pseudotime marching of the harmonic balance equations should be expected to reproduce periodic URANS solutions even in the case of strong nonlinearities.

It should be emphasized, however, that our argument assumes that the flow residual R is time-local and all the ingredients to compute it, in particular boundary conditions, are consistent for the semi-discrete URANS equations and the pseudotime HB solver. The argument above therefore suggests that a major difference between the pseudotime dynamics of the harmonic balance solver and the transients of the time-integration results can be due to different formulations of inlet and outlet boundary conditions. These are usually nonlocal in time, i.e., the residual R is not just a function of t and the current flow $q(t)$ but also involves the solutions at different pseudotime and/or time instants (τ', t'), $\tau' \leq \tau$. In our experience, the implementation of robust nonreflecting spectral boundary conditions is a rather intricate task and the measures to formulate a stable method are quite different for time integration schemes [22] than for harmonic balance methods [23]. Similar

considerations apply to the periodic phase-lag boundary conditions which are nonlocal in time and require special treatment for the time integration solver to prevent robustness issues [24].

The pseudotime solver discussed in this paper is formulated in the frequency domain and employs, like the steady solver, the Euler backward scheme to solve Eq. (4). Hence

$$\widehat{q}^{(m+1)} = \widehat{q}^{(m)} + \alpha \Delta \widehat{q}^{(m)} \tag{11}$$

where $\Delta\widehat{q}^{(m)}$ is an approximate solution to the linear equation

$$\left(\frac{1}{\Delta\tau} + \frac{\partial R^{\mathrm{HB}}}{\partial \widehat{q}}\Big|_{\widehat{q}^{(m)}} \right) \Delta\widehat{q}^{(m)} = -R^{\mathrm{HB}}(\widehat{q}^{(m)}). \tag{12}$$

To increase the robustness of the method, a relaxation factor of $\alpha < 1$ can be applied to the approximate solution of this system. The turbulence model equations are solved in a loosely coupled way, so there are five coupled conservation equations. The total number of real degrees of freedom of the harmonic balance system for the flow equations is thus

$$(2K+1) \times 5 \times \#\{\text{finite volume cells}\}.$$

Each higher harmonic consists of the real and imaginary components. With the mapping between real and imaginary components

Table 1 Real components of the vector of all harmonics

frequency	0	ω_1		ω_2		ω_3		...
real coefficient index	0	1	2	3	4	5	6	...

and harmonic indices outlined in Table 1, the Jacobian in Eqn.(12) has the form

$$\frac{\partial R^{\mathrm{HB}}}{\partial \widehat{q}} = \begin{pmatrix} 0 & 0 & 0 & \cdots & 0 & 0 \\ 0 & 0 & -\omega & \cdots & 0 & 0 \\ 0 & +\omega & 0 & \cdots & 0 & 0 \\ \vdots & \vdots & \vdots & \ddots & \vdots & \vdots \\ 0 & 0 & 0 & \cdots & 0 & -K\omega \\ 0 & 0 & 0 & \cdots & +K\omega & 0 \end{pmatrix} + \begin{pmatrix} * & * & * & \cdots & * & * \\ * & * & * & \cdots & * & * \\ * & * & * & \cdots & * & * \\ \vdots & \vdots & \vdots & \ddots & \vdots & \vdots \\ * & * & * & \cdots & * & * \\ * & * & * & \cdots & * & * \end{pmatrix}. \tag{13}$$

To stabilize the harmonic balance solver, a temporal damping is introduced by replacing the angular frequency ω with

$$\tilde{\omega} = \omega(1 - \mathbf{i}\varepsilon)$$

in the definition of the spectral time derivative. ε is typically set to a value in the range of $[0, 10^{-2}]$. The simulation results below were obtained with $\varepsilon = 10^{-3}$. On the left-hand side this modification means to substitute the k-th diagonal block in the first matrix of Eq. (13) with

$$k \begin{pmatrix} \varepsilon\omega & -\omega \\ +\omega & \varepsilon\omega \end{pmatrix}.$$

As is common practice the local pseudotime step size is computed from a global CFL number according to

$$\delta\tau_k = \frac{\mathrm{CFL}}{\lambda_{\max} + \omega_k},$$

where $\lambda_{\max}$ is an estimate of the maximal eigenvalue of the spatial discretization which, in turn, is computed from cell sizes and local flow conditions. Note that, slightly deviating from Eq. (12), the pseudotime step depends on the harmonic.

3.1 Computation of the Harmonic Balance System Jacobian. The definition in (1) can be rewritten as a matrix multiplication,

$$q_n = F^{\mathrm{inv}}_{nk} \widehat{q}_k \tag{14}$$

where $\widehat{q}$ is to be considered a real block vector (using the above correspondence), so F^{inv}_{nk} is a real 1×2 submatrix for $k > 0$. Similarly, F_{kn} is a 2×1 submatrix for $k > 0$. In terms of F and F^{inv}, the second summand of (13) is given by

$$\frac{\partial}{\partial \widehat{q}} \left(F R(F^{\mathrm{inv}} \widehat{q}) \right) = F \begin{pmatrix} \frac{\partial R}{\partial q}\Big|_{q_0} & 0 & \cdots & 0 \\ 0 & \frac{\partial R}{\partial q}\Big|_{q_1} & \cdots & 0 \\ \vdots & \vdots & \ddots & \vdots \\ 0 & 0 & \cdots & \frac{\partial R}{\partial q}\Big|_{q_{N-1}} \end{pmatrix} F^{\mathrm{inv}} \tag{15}$$

With this formula, one can readily compute the flow residual Jacobians during the sampling loop that is needed for the right-hand side of Eq. (12). Using F and F^{inv}, one computes the entries in the second matrix of Eq. (13) as

$$\frac{\partial \widehat{R(q)}_k}{\partial \widehat{q}_{k'}} = \sum_{n=0}^{N-1} F_{kn} \frac{\partial R}{\partial q}\Big|_{q_n} F^{\mathrm{inv}}_{nk'}. \tag{16}$$

for all harmonic indices k and k'. Each entry is a sparse matrix with a non-zero pattern that depends on the stencil necessary for the residual Jacobian. As the latter is approximated by the Jacobian of a first order accurate spatial scheme, the non-zero pattern is that of neighboring cells.

A naive way to implement the computation of each summand in Eq. (16) amounts to an effort that grows quadratically with the number of higher harmonics K. Since $N = n_{\mathrm{hh}}K + 1$, the computational effort for the computation of the complete left-hand side would thus grow with K^3. We can, however, exploit the fact that the multiplication with the residual Jacobian corresponds, in the frequency domain, to a convolution operator and can therefore be represented by a Toeplitz matrix if standard complex Fourier coefficients are used [25]. A matrix is called Toeplitz, if its diagonals are constant, i.e., its entries a_{ij} only depend on $i - j$. It is called Hankel, if its anti-diagonals are constant, i.e., if its entries only depend on $i + j$. In our representation the k-th harmonic corresponds to both the k-th and $-k$-th standard complex Fourier coefficient. Therefore, the flow residual Jacobian in the frequency domain is a sum of a Toeplitz and a Hankel matrix. To see this, observe that the Fourier matrix entries in Eq. (16) satisfy

$$F_{kn} F^{\mathrm{inv}}_{nk'} = \begin{cases} \frac{1}{2N} \left(e^{-2\pi\mathbf{i}\frac{n(k-k')}{N}} + e^{-2\pi\mathbf{i}\frac{n(k+k')}{N}} \mathscr{C} \right), & \text{if } k = 0, \\ \frac{1}{N} \left(e^{-2\pi\mathbf{i}\frac{n(k-k')}{N}} + e^{-2\pi\mathbf{i}\frac{n(k+k')}{N}} \mathscr{C} \right), & \text{if } k > 0. \end{cases} \tag{17}$$

Here, a complex number represents the complex multiplication with that number whereas $\mathscr{C}$ represents complex conjugation $z \mapsto \bar{z}$, the real representation of which is the matrix

$$\mathscr{C} = \begin{pmatrix} 1 & 0 \\ 0 & -1 \end{pmatrix}.$$

It follows that the matrix in Eq. (13) can be computed from the complex Fourier coefficients of the residual Jacobians,

$$\widehat{\left(\frac{\partial R}{\partial q} \right)}^{\mathbb{C}}_l = \frac{1}{N} \sum_{n=0}^{N-1} \left(\frac{\partial R}{\partial q}\Big|_{q_n} \right) e^{-\mathbf{i}\omega_l t_n}, \tag{18}$$

for $l \in [-\lfloor (N-1)/2 \rfloor, \lceil (N-1)/2 \rceil]$. The computational effort to compute these Fourier coefficients is proportional to K^2. Using this approach for the computation of the harmonic balance residual Jacobian, the computational effort grows only quadratically with the number of higher harmonics. Moreover, one can exploit the fact that the coefficient in Eq. (18) for $-l$ is the complex conjugate of the coefficient for l.

3.2 Simplified Harmonic Balance System Jacobian. Assume that the q_n do not vary strongly about the mean $\widehat{q}_0$. Then we can write $q_n = \widehat{q}_0 + q'_n$ and, assuming that the second derivatives of R w.r.t. q are bounded,

$$\left\| \frac{\partial R}{\partial q}\Big|_{q_n} - \frac{\partial R}{\partial q}\Big|_{\widehat{q}_0} \right\| = \mathrm{O}(\|q'\|_\infty). \tag{19}$$

Together with Eq. (16), this implies

$$\begin{aligned} \frac{\partial \widehat{R(q)}_k}{\partial \widehat{q}_{k'}} &= \sum_{n=0}^{N-1} F_{kn} \left(\frac{\partial R}{\partial q}\Big|_{\widehat{q}_0} + \frac{\partial R}{\partial q}\Big|_{q_n} - \frac{\partial R}{\partial q}\Big|_{\widehat{q}_0} \right) F^{\mathrm{inv}}_{nk'} \\ &= \sum_{n=0}^{N-1} F_{kn} \frac{\partial R}{\partial q}\Big|_{\widehat{q}_0} F^{\mathrm{inv}}_{nk'} + \mathrm{O}(\|q'\|_\infty) \\ &= \delta_{kk'} \frac{\partial R}{\partial q}\Big|_{\widehat{q}_0} + \mathrm{O}(\|q'\|_\infty) \end{aligned} \tag{20}$$

It follows that the left-hand side entries of the implicit system in Eq. (12) for $k \neq k'$ are bounded by a constant multiple of the unsteady amplitudes $\|q'\|_\infty$. Moreover, the diagonal entries can be approximated up to first order using

$$\frac{1}{\Delta\tau} + \mathbf{i}\omega k + \frac{\partial \widehat{R(q)}_k}{\partial \widehat{q}_k} \approx \frac{1}{\Delta\tau} + \mathbf{i}\omega k + \frac{\partial R}{\partial q}\Big|_{\widehat{q}_0}. \tag{21}$$

In contrast to the exact HB residual Jacobian, this is a complex linear matrix for each k. This approximation considerably reduces both the memory requirements and the computational effort of one pseudotime iteration since:

- The matrices for the different harmonics differ only by a constant diagonal.
- The second summand of Eq. (21) is computed just once per pseudotime step, outside the sampling loop.
- All matrix vector operations now grow only linearly with K.
- The implicit equations for the harmonics decouple.
- One can employ complex arithmetics.

It should be stressed again that the deviation of the simplified Jacobian from the fully coupled one scales with unsteady amplitudes. If the harmonic balance solver is used to predict effectively linear problems such as the onset of flutter on the basis of very small prescribed vibration amplitudes, this simplification should be expected to have a negligible impact on the convergence while the CPU costs are reduced considerably.

3.3 Linear Solvers. In recent years, a linear solver library for large block sparse systems has been integrated in TRACE. This library called Spliss (Sparse linear systems solver) [26] has been designed to target the demands of large-scale computational fluid dynamics (CFD) simulations, emphasizing node-level performance, computational accelerators [27], and scalability. The architecture of Spliss is characterized by its inherent flexibility, enabling the combination of various solution methods and preconditioners. Notable among these are the Jacobi method, SSOR (Successive Symmetric Overrelaxation), ILU (Incomplete LU Factorization), and a spectrum of Krylov methods, especially GMRES (Generalized Minimal Residual), line-implicit methods and multigrid.

A distinctive feature of Spliss lies in its tailored matrix type designed to exploit the simplified Jacobian structure of the harmonic balance systems with left-hand sides as in Eq. (21). This structure combines complex block-diagonals and real-valued off-diagonals, with an efficient utilization of the Single Instruction Multiple Data (SIMD) capabilities featured by modern processors [28].

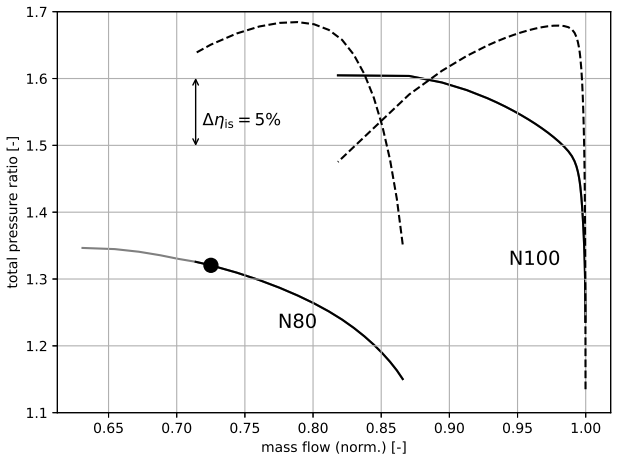

Fig. 2 Total pressure ratio and isentropic efficiency over mass flow of the TCD stage at 80% and 100% rotational speed.

4 Application

To demonstrate the capabilities the implicit solution methods above to simulate unsteady flow in off-design conditions, the solver has been applied to the Transonic Compressor Darmstadt (TCD) test case. For this compressor, experimental investigations are currently conducted at the Technical University of Darmstadt (TUDa) within the framework of the European research project ARiAS (Advanced Research into Aeromechanical Solutions). These studies have a strong focus on forced response vibrations of the blisk rotor [29]. The investigated 1.5-stage configuration comprises a wake generator, a blisk rotor designed by MTU Aero Engines, and a stator with 29 vanes, designed by TUDa and DLR (see [30]).

The configuration studied in this work has a wake generator with 8 prismatic NACA airfoils. The following harmonic balance simulations are carried out for an operating point on the 80% speedline which is marked with a dot in Fig. 2. Both speedlines has been computed with the steady solver using the whole configuration as computational domain, though the plot in Fig. 2 shows performance data for the stage only. The operating point considered is close to the numerical stall boundary, i.e., the steady solver no longer converges to a satisfactory residual level if the backpressure is further increased. The axial component of the wall shear stress along the suction side is depicted in Fig. 3 which shows a separated flow region close to the leading edge in the lower part of the blade. The computational domain for the harmonic balance simulations consists of one rotor passage. The modal gust boundary conditions [21] are employed at the rotor inlet to prescribe disturbances coming from the wake generator. The engine orders are thus integer multiples of 8. Three harmonics (m = 8, 16, 24) are used to resolve the unsteady flow in the rotor. Here, we apply the circumferential modes extracted from a Fourier decomposition of the outflow of the wake generator. The circumferential distribution of the axial velocity obtained from the reconstruction with the three mode orders given is plotted in Fig. 4. Here, the sec-

ond disturbance plotted ("scaled") corresponds to the same Fourier coefficients as in the original wake generator outflow, but the disturbance amplitudes are increased by a scaling factor of 8. The solver convergence will be assessed by the convergence of the first modal force harmonic for the eigenmode depicted in Fig. 5. The unsteady flow for the strong disturbance is shown in Fig. 6 at four time instants.

To assess the convergence of the solver, $L1$ residuals (averaged over all harmonics, conservation equations, and cells) as well as the modal force for the eigenmode depicted in Fig. 5 have been plotted in Fig. 7. The linear solution method for all results plotted in Fig. 7 was a preconditioned GMRES method with 50 iterations and ILU as preconditioner. For the original disturbances and using a CFL number of 10, the implicit HB solver converges within a few hundred iterations to a satisfactory level, both in terms of the residual and the modal force variation. One can see that, for this amplitude, discarding the coupling between the harmonics has almost no impact on the residual reduction per iteration.

When the disturbance amplitudes are scaled by a factor 8, however, the uncoupled Jacobian approach causes the solver to diverge, even with a CFL number as small as unity. In contrast, if the full Jacobian is used the implicit solver is robust for CFL numbers as high as 20. The residual reduction is not perfect though. The remaining residual level is considerably higher than in the original setup (even if the original residuals were scaled by a factor of 8). This indicates that due to non-linearity the pseudotime dynamics are qualitatively different for the two amplitudes. Observe that the convergence of the modal forces is satisfactory for the robust setups. In the fully coupled simulations with increased amplitudes, the relative variation is below 10^{-2} after less than 400 pseudotime steps. The normalization in Fig. 7(*b*) is increased by 8 for the high amplitude simulations. Hence, if the system response were linear, the normalized modal forces would all equal unity. The unsteady flow field in Fig. 6 shows that the position and strength of the shock oscillate strongly.

On the one hand, the results illustrate that the uncoupled Jacobian approach is applicable to numerically delicate operating points close to the numerical stall margin. On the other hand, the applicability is confined to a limited range of unsteady nonlinearity and it may be necessary to include the coupling between harmonics to be able to treat disturbances such as large shock oscillations.

The plots in Fig. 7 were all produced with preconditioned GMRES as linear solver with 50 iterations and ILU as preconditioner. The reason behind the choice for this rather powerful yet expensive linear solver was that it enables us to focus on the question

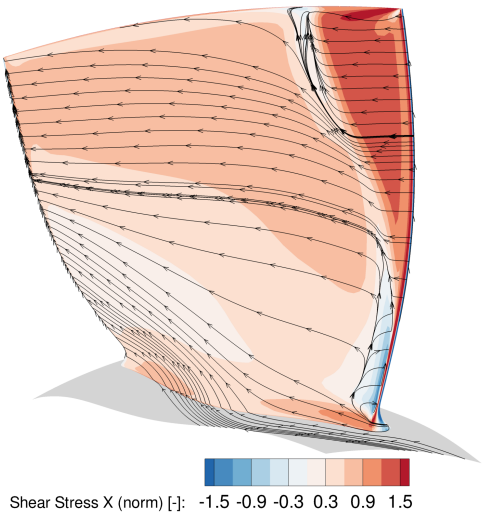

Fig. 3 Axial component of normalized wall shear stress along the rotor suction side.

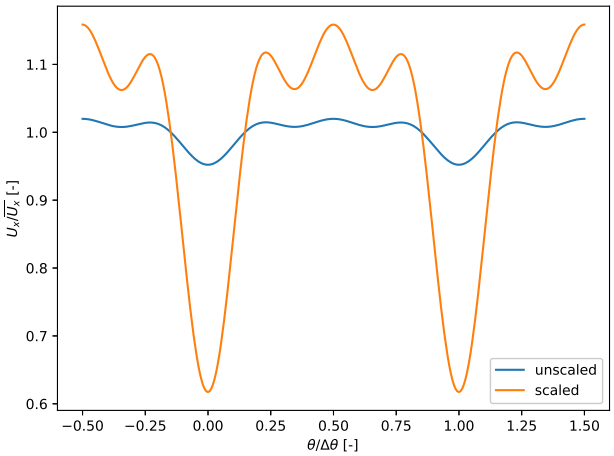

Fig. 4 Axial velocity disturbance along 80% channel height at rotor entry with three harmonics. Original IGV outflow and disturbance increased by a factor of 8.

whether the coupling between harmonics is needed. Note that even for the crashing simulation, the linear L2 residual reduction provided by GMRES during one pseudotime step was at least 8 orders of magnitude. We conclude from this that the robustness issues of the uncoupled solver, observed for the high disturbance amplitudes, cannot be remedied by simply switching to a more accurate approximate linear solution method.

When the harmonic coupling is taken into account, one can also use a rather cheap linear approximate solver such as SGS with one forward and one backward sweep. As the plot in Fig. 8 shows, with a moderate CFL number of 5, the SGS solver is robust and roughly as fast as the GMRES approach in terms of overall times to convergence.

When a simple linear solver is used and the left-hand side is recomputed in every pseudotime step the time spent during the computation of the matrix is significant. E.g., when using SGS with one sweep then the fast computation of the fully-coupled left-hand side reduces the overall CPU times by a factor of about 2.9 compared with what was called above the “naive” approach. Note that this speed-up factor increases with the number of higher harmonics (here $K = 3$) but decreases when a computationally expensive solution method (e.g. GMRES with many iterations) is used. The uncoupled approach, in turn, is about 11 times faster per pseudotime step (measured with one SGS sweep) than the fully

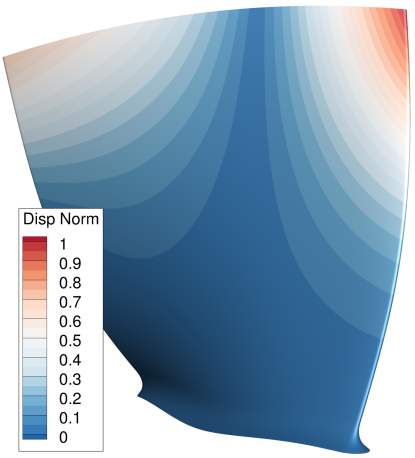

Fig. 5 Displacement vector norm of blade eigenmode.

coupled solver. Here, it should be mentioned that the implementation of the uncoupled approach has been improved over recent years so that it exploits the potentials in CPU cost savings that were listed in the previous section. In the fully coupled approach as it is implemented here, still $(K+1)^2$ residual Jacobians with 10 degrees of freedom (5 for the 0-th harmonic) per cell are stored even though the amount of information of the fully coupled system matrix has been shown above to reduce to only N residual Jacobians with 5 degrees of freedom per cell. Hence, the considerable speed-up factor could, at least to some extent, be due to the fact that, algorithmically, the two approaches have not been equally optimized.

4.1 Harmonic convergence. All computations above have been carried out with three harmonics, which, in view of the highly nonlinear flow response, seems a relatively coarse temporal resolution for the increased amplitude. To address the issue of harmonic convergence two additional setups have been simulated. The first one is a harmonic balance simulation with five harmonics. It uses GMRES with a CFL number of 20 since this was found to be the most efficient approach for three harmoncs. Otherwise this setup is identical to the coupled setup with three harmonics. The second one is a time-domain simulation with second-order backward differencing (BDF2) and 128 time steps per period. This simulation employs dual time stepping with 40 inner pseudotime steps and a pseudotime CFL number of 200. It should be pointed out that in order to achieve consistent results in the frequency and time domains, one has to use consistent inlet and outlet boundary conditions. For the test case here, consistent two-dimensional non-reflecting boundary conditions [22,31] with modal gusts for three circumferential mode orders (see Fig. 4) have been used. Since the interblade phase angle of the disturbance is 180°, we can achieve periodicity for the time-domain simulations by simulating a computational domain that comprises two passages. The resulting amplitude of the first modal force harmonic (normalized as before) is plotted over CPU time in Fig. 9. Figure 9(*a*) shows that, compared with the HB setup with three harmonics, the more accurate simulations give very similar results with relative discrepancies in terms of the modal force harmonic below 1%. This shows that from a practical point of view, three harmonics is a reasonable choice even for strongly nonlinear problems such as the high amplitude disturbance discussed here.

Figure 9(*b*) shows an estimate of the relative error of the modal force harmonic defined as follows. Suppose that $\widehat{f}_{\omega,i}$ is the current value of the modal force harmonic for the i-th (pseudo) time step. Note that for the time-domain simulation this value is an integral over the past 128 time steps. Then,

$$\overline{(\widehat{f}_{\omega,i'})_{i'\geq i}}$$

is the average of the time series of the values after the i-th step. To compare convergence speeds, we define an estimate of the instantaneous error by

$$\varepsilon_i = \|(\widehat{f}_{\omega,i'})_{i'\geq i} - \overline{(\widehat{f}_{\omega,i'})_{i'\geq i}}\|_\infty.$$

Note that this is just an estimate for the error due to non-convergence. As can be seen in Figure 9(*b*), increasing the number of harmonics in the HB solver has a moderate impact on the CPU costs. The time-domain simulation, however, takes considerably longer to reduce the modal force error to, say, 1%. For this setup, HB with three harmonics is roughly one order of magnitude faster than the time-domain approach. Note that this is only a rough estimate, since neither the harmonic balance nor the time-domain setups have been optimized for CPU time and modal force errors.

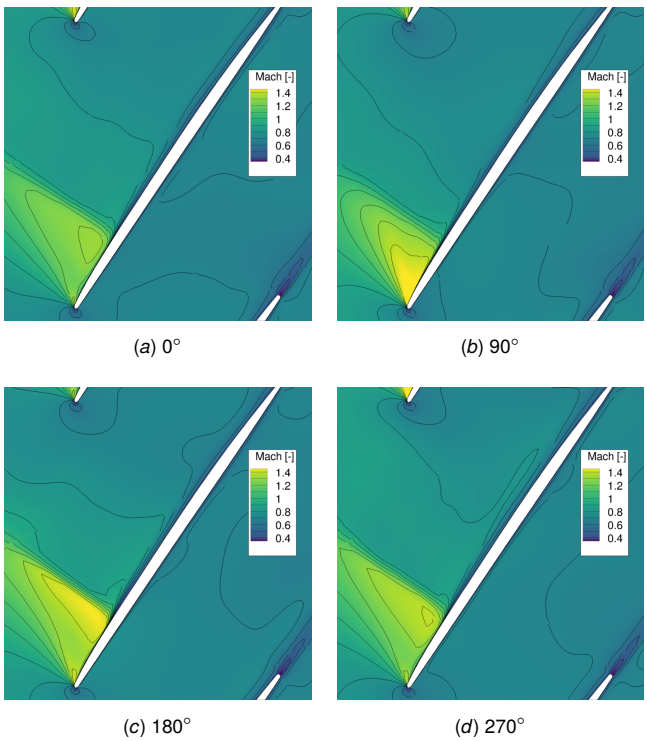

(*a*) 0° (*b*) 90°

(*c*) 180° (*d*) 270°

Fig. 6 Relative Mach number at 80% channel height at four phase positions.

5 Conclusions

Although the pseudotime marching approach for the harmonic balance equations lacks the physical, albeit heuristic, rationale of steady pseudotime solvers, it has been shown in this paper that it can be motivated by sound mathematical reasoning. The pseudotime solver should, in principle, be able to predict the same periodic flow solutions as the time-domain URANS approach. This motivates the pursuit of robust and efficient pseudotime marching formulations. Implicit methods are known for their robustness and should therefore be the method of choice.

The computation of the implicit system matrix in the frequency domain, if coded in a naive way, can become quite costly in terms of CPU time. However, the computations can be accelerated by exploiting the Toeplitz property of the matrix. Furthermore, it is shown that, in order to obtain an efficient method, one can simplify the implicit harmonic balance system for moderate amplitude disturbances. This simplification assumes that the variation of the flow residual Jacobian over the period is small. As a result, the harmonics decouple in the implicit linear system which leads to considerable CPU time savings if the implicit solver is formulated in the frequency domain.

The applicability of the simplifying assumption about approximately constant flow residual Jacobians is demonstrated for a transonic compressor at an operating point near the numerical stall boundary. It is shown that for an incoming disturbance derived from the outflow of a wake generator, the pseudotime solver is robust and the assumption of decoupled harmonics can be employed. However, as the disturbance amplitude is increased, the flow response becomes highly nonlinear and the simplified Jacobian leads to robustness issues, which cannot be overcome with a more powerful approximate linear solver. Instead, the linear system matrix itself must account for the time variation of the flow and the residual. On the one hand, the example shows that the simplifying assumption restricts the applicability of the solver to a limited range of nonlinearity. Thus, an implicit method that takes the interaction of the harmonics into account is needed for problems involving, for example, strong shock oscillations. On the other hand, the increased amplitude configuration should be considered as extreme. In the authors' experience, most applications

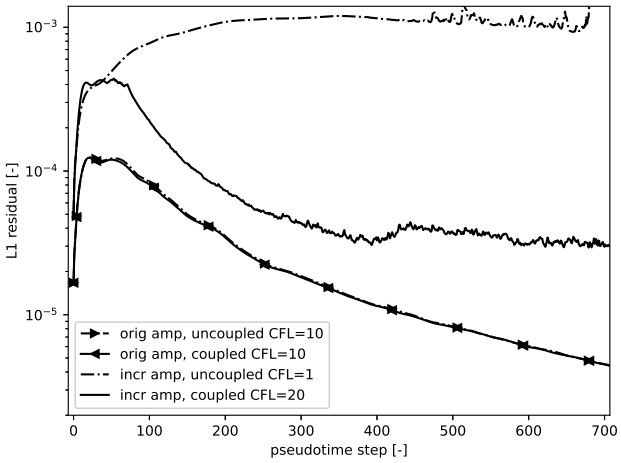

(*a*) L1 residual

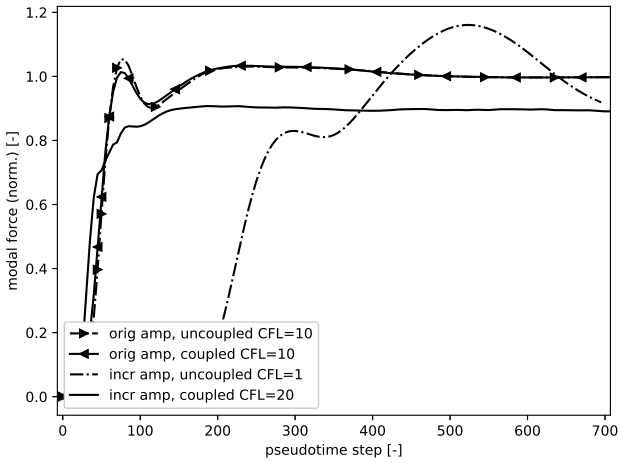

(*b*) modal force

Fig. 7 L1 residual and normalized modal force over pseudotime step. Original and increased amplitudes.

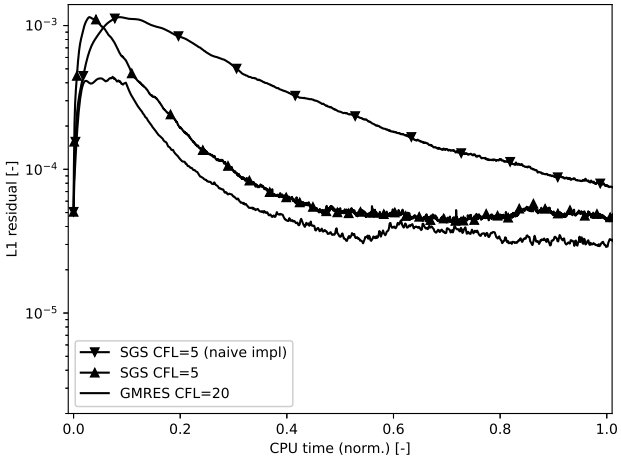

(*a*) L1 residual

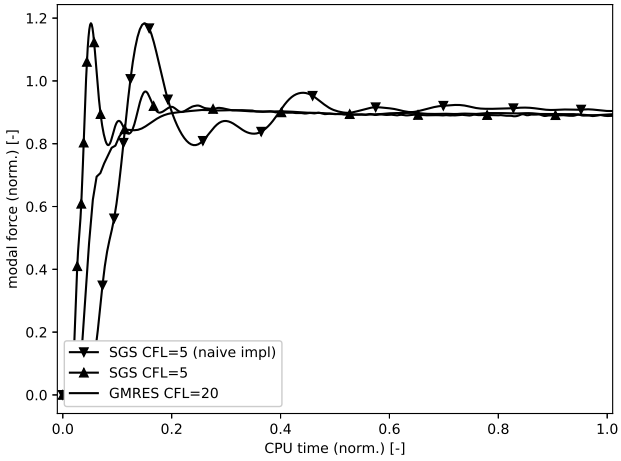

(*b*) modal force

Fig. 8 L1 residual and normalized modal force over normalized CPU time. Increased amplitude. Coupled Harmonics.

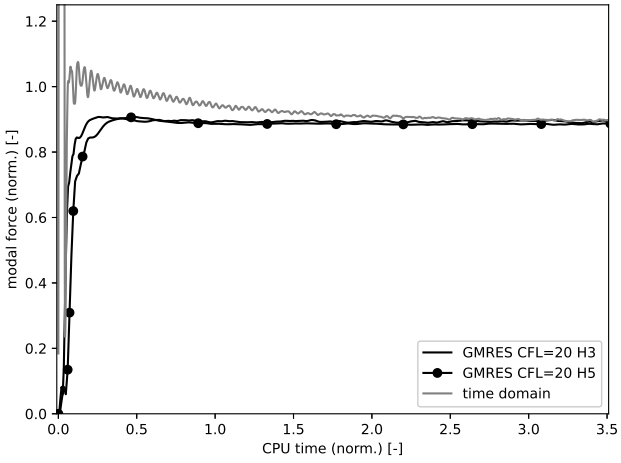

(*a*) modal force

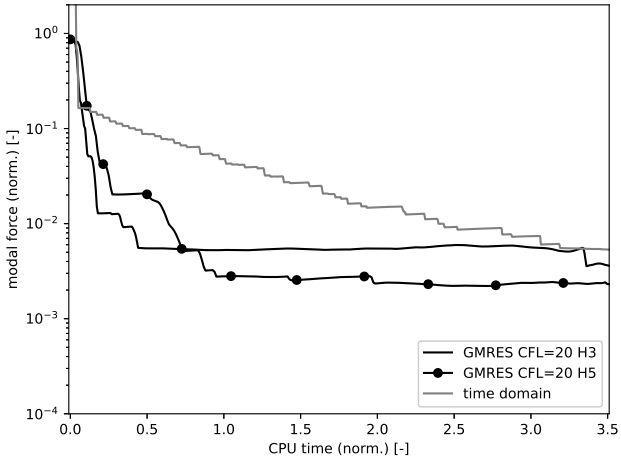

(*b*) modal force error

Fig. 9 Modal force and its variation over normalized CPU time. Increased amplitude. HB (3 and 5 harmonics) vs time domain solver.

can be treated with the simplified linear system matrix. Since the savings of the overall computational times can be considerable, it would therefore be desirable to derive a measure for the degree of nonlinearity and a criterion when the additional effort of the full coupling is necessary.

Acknowledgment

The authors acknowledge the financial support by the Federal Ministry for Economic Affairs and Climate Action of Germany in the framework of the joint project DigITecT (grant number 03EE5117A) which is part of the research corporation *AG Turbo*.

Nomenclature

$\mathbf{i}$ = square root of -1
k = harmonic index
m = pseudotime step index
n = sampling point index
n_{hh} = number of sampling points for the highest harmonic
q = flow state
$\widehat{q}_k$ = k-th flow harmonic
q_n = flow at n-th sampling point
t = (physical) time
t_n = n-th sampling point
Δt = time period
$\bar{z}$ = complex conjugate of z
$\mathscr{C}$ = complex conjugation operator
D_t = spectral time derivative
F = discrete Fourier transform
F^{inv} = inverse discrete Fourier transform
K = number of higher harmonics
N = number of sampling points
R = flow residual
R^{HB} = harmonic balance residual
$\mathrm{Re}\, z, \mathrm{Im}\, z$ = real and imaginary parts of z

Greek letters

δq = disturbance of q
τ = pseudotime
$\Delta\tau$ = pseudotime step
ω_k = angular frequency
Π_K = modal projection

References

[1] Hall, K. C., Thomas, J. P., and Clark, W. S., 2002, "Computation of Unsteady Nonlinear Flows in Cascades Using a Harmonic Balance Technique," AIAA J., **40**(5), pp. 879–886.

[2] Gilmore, R. J. and Steer, M. B., 1991, "Nonlinear circuit analysis using the method of harmonic balance - A review of the art. Part I. Introductory concepts," International Journal of Microwave and Millimeter-Wave Computer-Aided Engineering, **1**(1), pp. 22–37.

[3] Gilmore, R. J. and Steer, M. B., 1991, "Nonlinear circuit analysis using the method of harmonic balance - A review of the art. II. Advanced concepts," International Journal of Microwave and Millimeter-Wave Computer-Aided Engineering, **1**(2), pp. 159–180.

[4] Krack, M. and Gross, J., 2019, *Harmonic Balance for Nonlinear Vibration Problems*, Mathematical Engineering, Springer International Publishing, Gewerbestrasse 11, 6330 Cham, Switzerland.

[5] Woodgate, M. A. and Badcock, K. J., 2009, "Implicit Harmonic Balance Solver for Transonic Flow with Forced Motions," AIAA Journal, **47**(4), pp. 893–901.

[6] Su, X. and Yuan, X., 2010, "Implicit solution of time spectral method for periodic unsteady flows," International Journal for Numerical Methods in Fluids, **63**(7), pp. 860–876.

[7] Sicot, F., Dufour, G., and Gourdain, N., 2012, "A Time-Domain Harmonic Balance Method for Rotor/Stator Interactions," J. Turbomach., **134**(1), p. 011001.

[8] Thomas, J. P., Custer, C. H., Dowell, E. H., Hall, K. C., and Corre, C., 2013, "Compact Implementation Strategy for a Harmonic Balance Method Within Implicit Flow Solvers," AIAA Journal, **51**(6), pp. 1374–1381.

[9] Frey, C., Ashcroft, G., Kersken, H.-P., and Voigt, C., 2014, "A Harmonic Balance Technique for Multistage Turbomachinery Applications," *ASME Turbo Expo 2014: Turbine Technical Conference and Exposition*, Düsseldorf, Germany, June 16–20, 2014, Paper No. 45615, p. V02BT39A005.

[10] Gövert, S., Lipkowicz, J. T., and Janus, B., 2023, "Compressible Large Eddy Simulation of Thermoacoustic Instabilities in the PRECCINSTA Combustor Using Flamelet Generated Manifolds With Dynamic Thickened Flame Model," Journal of Engineering for Gas Turbines and Power, **146**(1), p. 011011.

[11] Engels-Putzka, A., Backhaus, J., and Frey, C., 2019, "Forced Response Sensitivity Analysis Using an Adjoint Harmonic Balance Solver," Journal of Turbomachinery, **141**(3), pp. 031014–031014–8.

[12] Bergmann, M., Morsbach, C., Klose, B. F., Ashcroft, G., and Kügeler, E., 2023, "A Numerical Test Rig for Turbomachinery Flows Based on Large Eddy Simulations With a High-Order Discontinuous Galerkin Scheme—Part I: Sliding Interfaces and Unsteady Row Interactions," Journal of Turbomachinery, **146**(2), p. 021005.

[13] Roe, P. L., 1981, "Approximate Riemann solvers, parameter vectors, and difference schemes," J. Comput. Phys., **43**(2), pp. 357 – 372.

[14] van Leer, B., 1979, "Towards the ultimate conservative difference scheme. V. A second-order sequel to Godunov's method," J. Comput. Phys., **32**(1), pp. 101 – 136.

[15] van Albada, G. D., van Leer, B., and Roberts, W. W., Jr., 1982, "A comparative study of computational methods in cosmic gas dynamics," Astron. Astrophys., **108**(1), pp. 76–84.

[16] Wilcox, D. C., 1988, "Reassessment of the Scale-Determining Equation for Advanced Turbulence Models," AIAA J., **26**(11), pp. 1299–1310.

[17] Kato, M. and Launder, B. E., 1993, "The Modeling of Turbulent Flow Around Stationary and Vibrating Square Cylinders," *9th Symposium on Turbulent Shear Flows*, Kyoto, Japan, August 16–18, 1993, pp. 10.4.1–10.4.6.

[18] Orszag, S. A., 1971, "Elimination of aliasing in finite-difference schemes by filtering high-wavenumber components," J. Atmos. Sci., **28**, p. 1074.

[19] Frey, C., Ashcroft, G., Kersken, H.-P., Schönweitz, D., and Mennicken, M., 2018, "Simulation of Indexing and Clocking with Harmonic Balance," Int. J. Turbomach. Propuls. Power, **3**(1).

[20] Junge, L., Frey, C., Ashcroft, G., and Kuegeler, E., 2021, "A New Harmonic Balance Approach Using Multidimensional Time," Journal of Engineering for Gas Turbines and Power, **143**(8), p. 081007.

[21] Frey, C., Ashcroft, G., and Kersken, H.-P., 2015, "Simulations of Unsteady Blade Row Interactions Using Linear and Non-Linear Frequency Domain Methods," *ASME Turbo Expo 2015: Turbine Technical Conference and Exposition*, Vol. 2B: Turbomachinery, Montreal, Quebec, Canada, June 15–19, 2015, Paper No. 56642, p. V02BT39A037.

[22] Schlüß, D. and Frey, C., 2019, "Time domain implementation of a spectral non-reflecting boundary condition for unsteady turbomachinery flows," *24th ISABE Conference*, Canberra, Australia, 22-27 September 2019, https://elib.dlr.de/132881/

[23] Frey, C., Schlüß, D., Wolfrum, N., Bechlars, P., and Beck, M., 2020, "On the formulation of nonreflecting boundary conditions for turbomachinery configurations: Part I-Theory and implementation," *Proceedings of the ASME Turbo Expo*, Vol. 2C, Virtual Conference, September 21 – 25, 2020, doi: 10.1115/GT2020-14684.

[24] Li, H. D. and He, L., 2002, "Single-Passage Analysis of Unsteady Flows Around Vibrating Blades of a Transonic Fan Under Inlet Distortion," Journal of Turbomachinery, **124**(2), pp. 285–292.

[25] Leung, A. Y. T. and Ge, T., 1995, "Toeplitz Jacobian Matrix for Nonlinear Periodic Vibration," Journal of Applied Mechanics, **62**(3), pp. 709–717.

[26] Krzikalla, O., Rempke, A., Bleh, A., Wagner, M., and Gerhold, T., 2021, "Spliss: a sparse linear system solver for transparent integration of emerging HPC technologies into CFD solvers and applications," *STAB/DGLR Symposium 2020: New Results in Numerical and Experimental Fluid Mechanics XIII, pp 635–645*, A. Dillmann, G. Heller, E. Krämer, and C. Wagner, eds., Springer International Publishing, Cham, pp. 635–645, doi: 10.1007/978-3-030-79561-0_60.

[27] Mohnke, J. and Wagner, M., 2023, "A Look at Performance and Scalability of the GPU Accelerated Sparse Linear System Solver Spliss," *29th International Conference on Parallel and Distributed Computing*, Springer Nature Switzerland, Ocean Flower Island, China, 17-21 December 2023, pp. 637–648, doi: 10.1007/978-3-031-39698-4.

[28] Kühn, M. J., Holke, J., Lutz, A., Thies, J., Röhrig-Zöllner, M., Bleh, A., Backhaus, J., and Basermann, A., 2023, "SIMD vectorization for simultaneous solution of locally varying linear systems with multiple right-hand sides," The Journal of Supercomputing, **79**(13), pp. 14684–14706.

[29] Kilian, N., Klausmann, F., Franke, D., Schiffer, H.-P., and Gutiérrez Salas, M., 2022, "Numerical investigation of forced response in a transonic compressor stage - highlighting challenges using experimental validation," *16th International Symposium on Unsteady Aerodynamics Aeroacoustics and Aeroelasticity of Turbomachines (ISUAAAT)*, Toledo, Spain, September 19-23 2022, (to appear).

[30] Bakhtiari, F., Wartzek, F., Leichtfuß, S., Schiffer, H.-P., Goinis, G., and Nicke, E., 2015, "Design and optimization of a new stator for the transonic compressor rig at TU Darmstadt," *Deutscher Luft- und Raumfahrtkongress 2015*, Rostock, Germany, 22-24 September 2015.

[31] Schlüß, D., Frey, C., and Ashcroft, G., 2016, "Consistent Non-reflecting Boundary Conditions For Both Steady And Unsteady Flow Simulations In Turbomachinery Applications," *ECCOMAS Congress 2016 VII European Congress on Computational Methods in Applied Sciences and Engineering*, Crete, Greece, 5-10 June 2016, https://eccomas2016.org/proceedings/pdf/5411.pdf

List of Figures

List of Tables